ACS APPLIED MATERIALS & INTERFACES

Research Article

www.acsami.org

Synthesis of Graphene Oxide Based CuO Nanoparticles Composite Electrode for Highly Enhanced Nonenzymatic Glucose Detection

Jian Song,[†] Lin Xu,*[,†] Chunyang Zhou,[†] Ruiqing Xing,[†] Qilin Dai,[†] Dali Liu,[†] and Hongwei Song*[,†,‡]

[†]State Key Laboratory on Integrated Optoelectronics, College of Electronic Science and Engineering, Jilin University, 2699 Qianjin Street, Changchun, 130012, People's Republic of China

[‡]The State Key Laboratory of Bioelectronics, Southeast University, 210096, People's Republic of China

Supporting Information

ABSTRACT: CuO nanoparticles (NPs) based graphene oxide (CuO/GO) composites with different CuO NPs loading amount as well as pure CuO NPs with different hydrothermal temperatures were synthesized using a hydrothermal method. Transmission electron microscopy (TEM), X-ray diffraction (XRD), thermogravimetric analysis (TGA), and Raman spectroscopy were employed to characterize the morphology and structures of our samples. The influence of hydrothermal temperature, GO sheet, and loading amount of CuO on particle size and structure of CuO was systemically investigated. The nonenzymatic biosensing properties of CuO/GO composites and CuO NPs toward glucose were studied based on glassy carbon electrode (GCE). The sensing properties of CuO NPs were improved after loading on GO sheets. The CuO/GO composites with saturated loading of the CuO NPs exhibited the best nonenzymatic biosensing behavior. It exhibited a sensitivity of 262.52 μA mM^{-1} cm^{-2} to glucose with a 0.69 μM detection limit (S/N = 3) and a linear range from 2.79 μM to 2.03 mM under a working potential of +0.7 V. It also showed outstanding long term stability, good reproducibility, excellent selectivity, and accurate measurement in real serum sample. It is believed that CuO/GO composites show good promise for further application on nonenzymatic glucose biosensors.

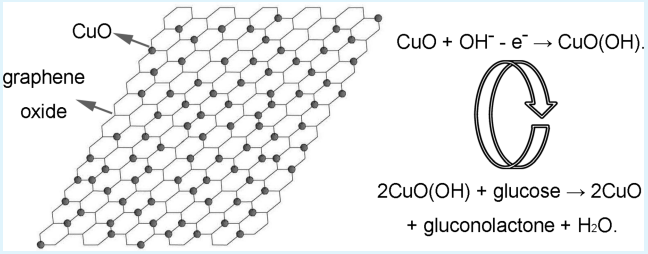

KEYWORDS: *graphene, CuO, hydrothermal procedure, composite, glucose detection*

1. INTRODUCTION

To accurately detect glucose is of immense scientific technological importance for clinical diagnostics in diabetes control and analytical applications in biotechnology, environmental pollution control, and the food industry.[1−3] Amperometric glucose sensor is a potential technology that can reach clinic glucose measurement accuracy. Since enzyme based amperometric sensors have the greatest drawback of poor stability because of inherent nature of enzymes,[4−6] many methods have been developed to determine glucose concentration without using them.[7−9] However, because of the surface poisoning from some adsorbed intermediates and chloride, most of nonenzymatic sensors have great problems with low sensitivity and poor selectivity which can be attributed to the adsorption of intermediates.[10,11] Generally, the blood glucose range is 3.6−7.5 and 1.1−20.8 mM for healthy people and diabetic patients, respectively. Hence, it is pertinent to explore and develop nonenzymatic sensors with high sensitivity and low detection limit to achieve convincing clinical measurements.

Graphene is composed of single-atom-thick planar carbon atoms that are arranged in a perfect honeycomb lattice sheet and has a zero band-gap.[12−14] The low noise level property of graphene is a great advantage for the detection of slight current changes induced by biological reactions.[5−17] In recent years, graphene-based hybrids bring new opportunities for nonenzymatic sensor performance because these hybrids afford significant physicochemical properties by effective adjustment or interaction of graphene sheets and incorporated materials.[18,19] Among these graphene-based hybrids, combining graphene with functional metal oxide semiconductor nanomaterials shows vast potential for nonenzymatic sensor application in clinical diagnostics.[9,20] CuO is a p-type semiconductor which always has better performance than others in nonenzymatic glucose sensing area. The reason can be attributed to the good electrochemical activity and the ability to promote electron transfer reactions.[21] Up to now, there are only a few studies about semiconductor/graphene nanocomposite materials for glucose detection based on the electrochemical method. For example, Luo et al. used an electrochemically deposited method to prepare copper oxide nanocubes and graphene nanocomposite modified GCE.[20] The linear range is from 2 μM to 4 mM with a detection limit of 0.7 μM (S/N = 3). Dong et al. prepared a 3D Co_3O_4/graphene electrode for nonenzymatic glucose detection. The corresponding sensitivity is 3.39 mA mM^{-1} cm^{-2}, but the linear range is only 0.1−80 μM.[9] However, there are limited instances to use CuO/graphene based

Received: August 22, 2013
Accepted: November 1, 2013
Published: November 1, 2013

nanocomposite materials to actually and accurately measure the glucose condition in human blood.

In this work, we loaded different amounts of CuO NPs on GO sheets through an in situ chemical synthesis approach.[22] In addition, pure CuO NPs obtained in different hydrothermal reaction temperatures were also prepared for comparison. Then they were employed on high performance nonenzymatic glucose sensing. Significant improvements were observed on the GO/CuO composite; moreover, the GO/CuO composite can also accurately measure human glucose in blood.

2. MATERIALS AND METHODS

2.1. Preparation of CuO/GO Composite and CuO Nanoparticles. The chemicals we used were all analytical grade and have not been further purified. GO sheets were bought from Nanjing XFNANO Materials Tech Co., Ltd., which were synthesized by a modified Hummers method.[23] CuO/GO composite was synthesized by using the method reported in a previous work.[24] Typically, an amount of 5 mg of GO was first dispersed in 5 mL of deionized water. Then the suspension was magnetically stirred for 1 h and sonicated for 5 h in order to disperse the GO uniformly in deionized water. All these procedures were performed under room temperature. The resulting suspension was mixed with 20 mL of *N*,*N*-dimethylformamide (DMF) and trickled into a round-bottom flask, then heated to 90°C with magnetic stirring. When the solution temperature reached 90 °C, an amount of 5 mL of DMF with different amounts of cupric acetate ($Cu(Ac)_2$, 4, 12, and 22 g/L which were named as S_1, S_2, and S_3, respectively) was then injected into the round-bottom flask. The mixture was kept at 90 °C for 1 h with stirring. Then the composite materials were collected (centrifugation and washed 3 times using deionized water) and then trickled into autoclaves after being dispersed in 30 mL of deionized water again. The hydrothermal reaction was performed for 10 h measured at different temperatures (120, 150, and 180°C). Finally, the product was collected after being washed by deionized water 3 times and the drying process. To further investigate the optimal loading amount of CuO on GO sheets, we synthesized the CuO/GO composite with a $Cu(Ac)_2$ content of 35 g/L, which was higher than that of S_3. Its cleanout fluid was very turbid even after washing it 2 times during the centrifugation and wash process. The cleanout fluid became clear after we washed it for 5 times. In addition, we also tested the nonenzymatic glucose properties of this composite and got a similar result with S_3 (the detail experimental data are not shown). So we can conclude that the loading capacity of GO sheets already reached saturation when the $Cu(Ac)_2$ content was 22 g/L (S_3). Moreover, the CuO NPs were synthesized with the same process with different hydrothermal reaction temperatures except the addition of GO for comparison.

2.2. Preparation of CuO/GO and CuO Modified Electrodes. First, the GCE (diameter of 3 mm) was polished by using 1 mm and 0.05 mm alumina slurries. Then the electrode was washed with nitric acid (0.2 M), acetone, ethanol, deionized water and dried at room temperature. For surface modification, 5 mg of CuO/GO was mixed with 1 mL of ethanol and sonicated for 1 h. After that, 5 μL of CuO/GO suspension was dropped onto the surface of GCE. In order to entrap the sample, 5 μL of Nafion solution (0.5 wt % in ethanol) covered it and drying in air was done. The as-prepared electrode (denoted as CuO/GO/GCE) needed to be wetted before use. We also made the pure CuO NPs or GO modified GCEs (denoted as CuO/GCE or GO/GCE, respectively) modified electrodes as comparison in a similar way.

2.3. Apparatus. The transmission electron microscope (TEM) images were measured on a JEM-2010 (Japan), and the working voltage is 200 kV. The high-resolution TEM (HRTEM) images and SAED patterns were measured on a JEOL-2100F high-resolution transmission electron microscope (Japan) with a working voltage of 200 kV. X-ray diffraction (XRD) patterns were recorded on a Rigaku D/max 2550 X-ray diffractometer, using a monochromatized Cu target radiation source (Japan). Thermogravimetric analysis (TGA) data were conducted on a SDT 2960 differential thermal analyzer (TA Instruments, New Castle, DE) at a heating rate of 10 °C/min in air. Resonance Raman spectra were conducted on an inVia H30434 Raman spectrophotometer (Renishaw, England). Cyclic voltammetry (CV) and current−time (I−t) measurements were recorded on a model CHI630D electrochemical analyzer (ChenHua Instruments Co. Ltd., Shanghai, China). All the electrochemical measurements were conducted using a three-electrode electrochemical cell, in which the as-modified GCE was used as working electrode, Ag/AgCl electrode was used as the reference electrode, and a platinum wire was used as the counter electrode. The working electrode is a glassy carbon electrode (diameter of 3 mm).

3. RESULTS AND DISCUSSION

3.1. Characterization of the CuO NPs and CuO/GO Composites. The morphology of the pure CuO NPs, GO sheets, and CuO/GO composites was first examined. Figure 1a

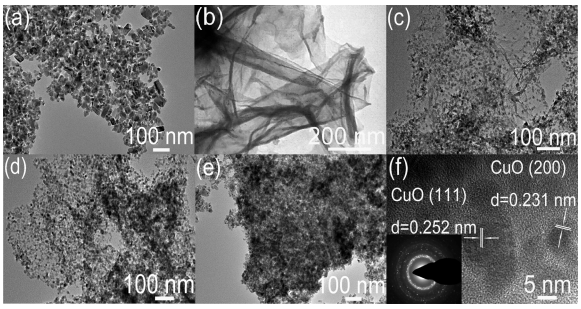

Figure 1. TEM images of (a) CuO NPs synthesized at 120 °C, (b) GO sheets, (c−e) CuO/GO composites based on S_1, S_2, and S_3 and (f) HRTEM image of CuO/GO composite based on S_3. The inset is the corresponding SEAD pattern.

(120 °C) and Figure S1 in Supporting Information (150 and 180°C) are the TEM images of pure CuO NPs synthesized under different hydrothermal reaction temperatures. It can be observed that the CuO products prepared at 120°C are irregular and prefer to aggregate together. The average size was estimated to be 25 nm. As the hydrothermal temperature increases from 120 to 180 °C, the CuO products become more homogeneous. The average size of CuO NPs also increases from 25 to 45 nm. Panel b of Figure 1 shows the morphology of GO nanosheets used in this work, and panels c−e of Figure 1 exhibit the morphology of the CuO/GO composites loaded with different amounts of CuO NPs when the hydrothermal reaction is 120 °C. In CuO/GO composites, because of the smooth and planar surface provided by GO sheets, the CuO can grow on GO sheets independently instead of aggregating together, and most of products demonstrate regular small NP morphology. As the loading amount of CuO NPs gradually increases, the CuO NPs become dense on the GO sheets (see Figure 1e). It should be highlighted that when the concentration of $Cu(Ac)_2$ was 22 g/L (S_3), the loading capacity of GO sheets reached saturation. Figure 1f shows the HRTEM image and SEAD pattern of CuO/GO composites (S_3). From the HRTEM image, the (111) and (200) faces of monoclinic CuO are observed and marked. The interplanar distances of the fringes are 0.252 and 0.231 nm, respectively. The inset of Figure 1f shows the corresponding SEAD pattern, which reveals that the CuO/GO composite sample yields a polycrystalline structure.

The structures of the pure CuO NPs prepared at different hydrothermal temperatures were identified by the XRD

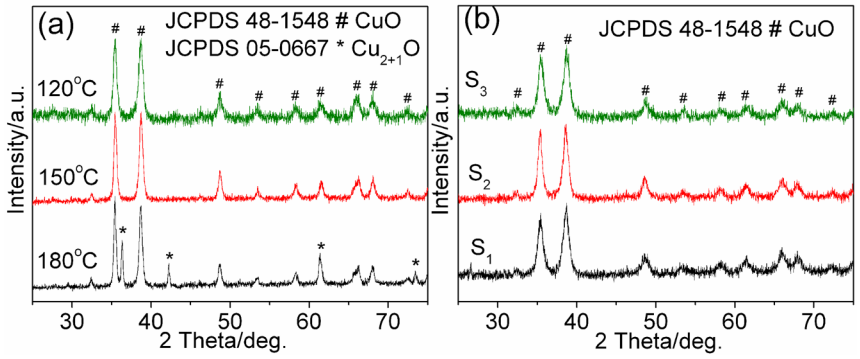

Figure 2. XRD patterns of (a) CuO NPs synthesized at different temperatures (120, 150, and 180 °C) and (b) CuO/GO composites S_1, S_2, and S_3.

patterns, as shown in Figure 2a. When the hydrothermal temperature is relatively high (180 °C in our work), two kinds of CuO XRD patterns appeared, which are indexed to the mixture of monoclinic CuO (JCPDS 48-1548, shown as #) and a small amount of cubic CuO (JCPDS 05-0667, shown as ∗). When the hydrothermal temperature decreases to 150 and 120°C, the impurity cuprite CuO phase disappears. It should be mentioned that for CuO/GO composites, hydrothermal reaction at 120 °C is important for obtaining CuO/GO composites with pure monoclinic CuO phase and good electrochemical performance as glucose sensor.[25] When the hydrothermal temperature is below 120 °C, the CuO/GO composite could hardly be formed. While the hydrothermal temperature is above 120°C (150 or 180°C), the electrochemical performance deteriorates (as proved below). Thereby, 120°C is chosen as the optimum temperature to synthesize the CuO/GO composite. Figure 2b shows the XRD patterns of CuO/GO composites synthesized at 120 °C. It can be seen that the XRD patterns of CuO/GO composites all show a strong monoclinic CuO phase.

To further confirm the thermal stability and the composition of CuO and GO in each CuO/GO composite sample, thermal behaviors were investigated through TGA. As shown in Figure 3, the mass loss below 150 °C (7.3%, 6.9%, and 4.8% for S_1, S_2, and S_3, respectively) can be attributed to the water and organic solvent attached on the materials. The mass loss around 200 °C increases to 8.2%, 7.4%, and 5.9% for S_1, S_2, and S_3, respectively, which is caused by the decomposition of residual oxygen-containing functional groups. As is calculated, the weight loss of the CuO/GO nanocomposites in the removal of residual oxygen functional group process gradually decreases, which can be ascribed to the elimination of oxygen-containing functional groups. Significant mass loss was detected when the CuO/GO nanocomposites were heated to 600 °C (30.5%, 20.8%, and 13.9% for S_1, S_2, and S_3, respectively). The reason can be attributed to the skeleton from GO.[26] There are no obvious mass loss when the CuO/GO nanocomposites are heated to 600°C; thus, the mass percentages of CuO in S_1, S_2, and S_3 are calculated to be 69.5%, 79.2%, and 86.1%, respectively.

The Raman spectra of GO and CuO/GO composites are shown in Figure 4. The D and G bands were observed in all

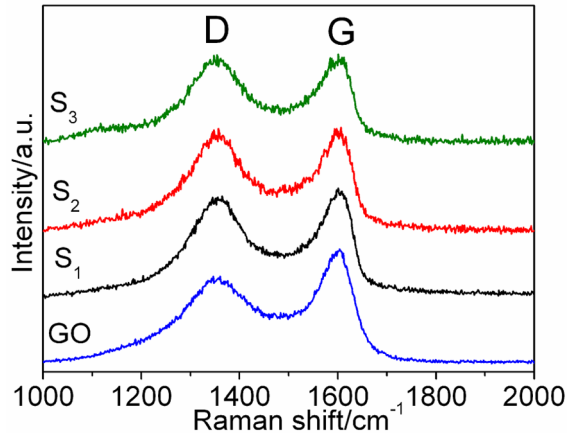

Figure 4. Raman spectra of GO and CuO/GO composites.

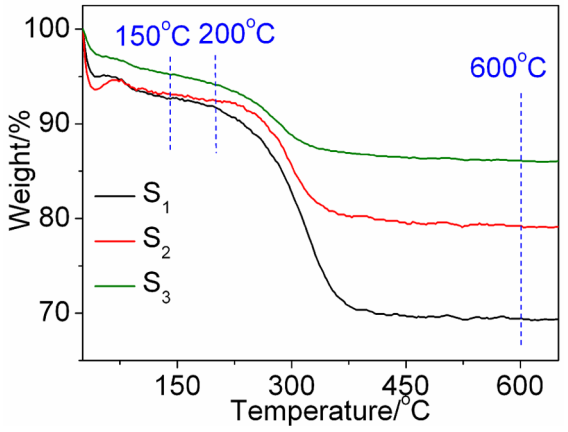

Figure 3. TGA curves of S_1, S_2, and S_3 samples.

samples in the range of 1000−2000 cm^{-1}. Generally in GO based samples, the disorder-induced D bands arise from the tangential stretch and sp^3-hybridized carbon and the G band represents the crystalline graphite with E_{2g} zone center mode;[26] moreover, the I_D/I_G ratio depends strongly on the amount of disorder in the graphitic material.[27] The I_D/I_G ratio should increase when more defects are introduced into GO. According to Figure 4, the I_D/I_G ratio of CuO/GO composite is 1.03 (S_3), 0.96 (S_2), and 0.87 (S_1), which is much higher than the 0.77 calculated from GO. That is to say, CuO modification can be effective in bringing a large amount of defects into the structure of GO.

3.2. Nonenzymatic Glucose Electrochemistry Behavior of CuO/GO/GCEs. The preliminary information on the electrochemical kinetics of CuO/GO/GCEs compared with CuO/GCEs was derived from cyclic voltammetry (CV) curves in 0.1 M NaOH solution, and the scan rate is 100 mV/s. First,

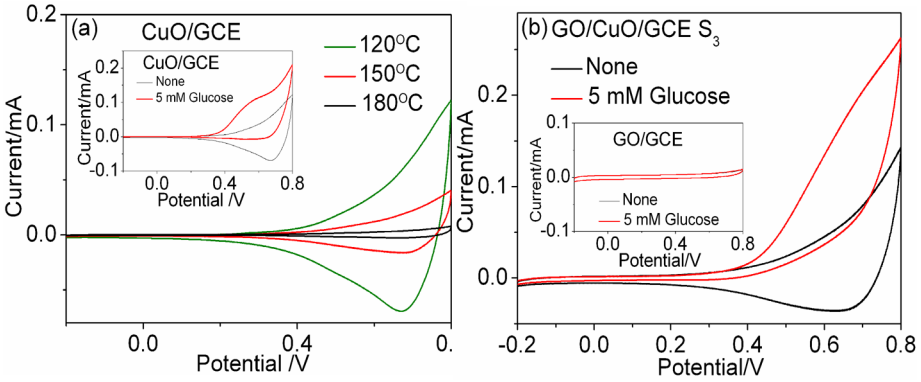

Figure 5. CV curves of (a) CuO NPs synthesized at 120, 150, and 180 °C. The inset is the CuO NPs synthesized at 120 °C in 0.1 M NaOH before (black trace) and after (red trace) the injection of 5 mM glucose. (b) CuO/GO composite S_3 and GO sheet (inset) in 0.1 M NaOH before (black trace) and after (red trace) the injection of 5 mM glucose.

the CV curves of three CuO/GCEs sensors were recorded. As shown in Figure 5a, a reduction peak corresponding to the potential of approximately +0.67 V vs Ag/AgCl was observed for all the three CuO/GCEs sensors. This peak corresponds to the Cu(II)/Cu(III) redox couple according to previous studies.[28,29] The corresponding reaction process is

$$CuO + OH^- - e^- \rightarrow CuO(OH)$$

The peak currents of the 120, 150, and 180 °C CuO NP samples are 69.5, 16.6, and 2.5 μA, respectively. This indicates that the CuO NPs obtained at 120°C can effectively accelerate the electron transfer, which is attributed to the increased surface to volume ratio of the CuO NPs compared with the other samples. The inset of Figure 5a presents the CVs before (shown in black trace) and after (shown in red trace) the injection of 5 mM glucose for CuO/GCE based on 120 °C CuO NPs. As can be seen, after the injection of glucose, the glucose oxidation peak can be easily observed at 0.48 eV, according to the following reactions:

$$2CuO(OH) + \text{glucose} \rightarrow 2CuO + \text{gluconolactone} + H_2O$$

The Cu(II)/Cu(III) redox couple is the essential factor for nonenzymatic electrochemical glucose detection. After the injection of glucose, electrons are transferred from glucose to the electrode. A Cu(III) ion obtains an electron and acts as an electron delivery system. The corresponding sensing mechanism schematic is shown in Scheme 1.

Figure 5b shows the CV curve of the CuO/GO/GCE sensor based on S_3 before and after the injection of 5 mM glucose, and the inset shows the CV curve of the GO/GCE sensor for comparison. Since no redox couple can be found on GO, GO should have no contribution to direct nonenzymatic glucose detection. According to Figure 5b, it can be observed that GO/GCE nearly has no response after addition of 5 mM glucose, indicating that GO is the indirect partner for the response of glucose. In contrast to the CuO/GCE sensor, the corresponding peak current of CuO/GO/GCE sensor based on S_3 largely increases. It should be highlighted that the CuO/GO/GCE sensors based on S_1 and S_2 also have improved response to glucose in comparison to CuO/GCE (see Figure S2); however, the responses of the CuO/GO/GCE sensors based on S_1 and S_2 are lower than that based on S_3.

The CV measurements of CuO/GO/GCE based on S_3 were further performed in 0.1 M NaOH solution at different scan rates of 50−100 mV/s after the injection of 1 mM glucose. As depicted in Figure 6, the redox peak currents changed linearly

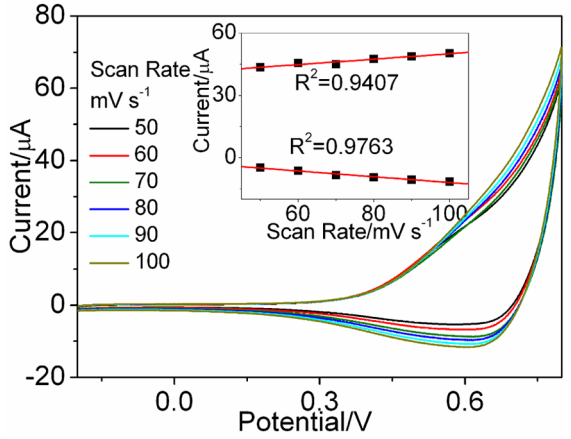

Figure 6. CV curves of CuO/GO composite based on S_3 in 0.1 M NaOH solution at various scan rates (50, 60, 70, 80, 90, and 100 mV/s). The inset is plots of peak current vs scan rate.

Scheme 1. Illustration of Nonenzymatic Glucose Sensing Mechanism by Using CuO/GO Composite

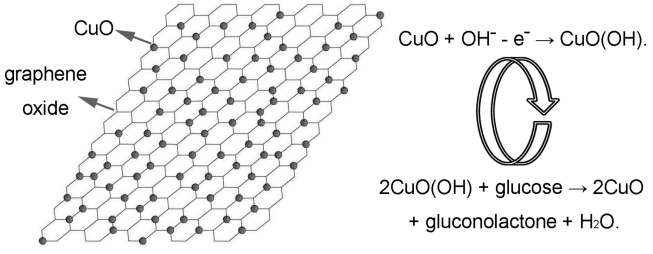

and excellent correlation coefficients are determined. The results indicate that the CuO/GO/GCEs are working under a surface-controlled electrochemical process in CuO/GO/GCEs.[9]

3.3. Amperometric Detection of Glucose at the Modified Electrodes. The current−time (I−t) curve was performed to determine the amperometric sensing property of CuO/GO/GCEs. The working potential is +0.7 V, and all measurements are taken in 0.1 M NaOH solution. First, the

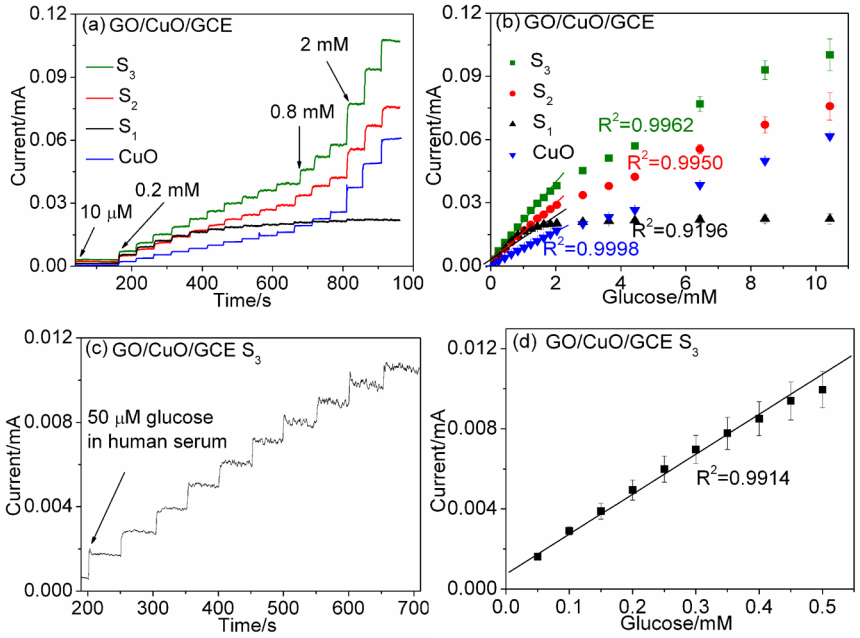

Figure 7. Amperometric responses: (a) CuO (120 °C), S_1, S_2, and S_3; (b) the corresponding calibration curves of (a); (c) S_3 to successive additions of human serum contained 50 μM glucose; (d) corresponding calibration curves of (c).

typical amperometric responses of CuO/GCEs based on CuO NPs with different hydrothermal temperatures by addition of different amount of glucose were obtained, as shown in Figure S3a. It is found that the 120 °C CuO NPs are more sensitive to the change of glucose concentration, which is consistent with the corresponding CV curves. The calibration curves for these three CuO/GCEs are shown in Figure S3b, and all these sensors display good linearity.

The $I-t$ curves of CuO/GCE (based on 120 °C CuO NPs) and CuO/GO/GCEs sensors based on S_1-S_3 samples by gradual addition of glucose were also measured. As shown in Figure 7a, the sensors produced an excellent amperometric response with a short response time. Furthermore, the corresponding responses of CuO/GO/GCEs sensors based on S_2 and S_3 are more obvious than those of CuO/GCEs. However, the response of CuO/GO/GCE sensor based on S_1 is lower than that of CuO/GCE. The calibration curves for the CuO/GO/GCEs are shown in Figure 7b, and the corresponding sensitivity, correlation coefficient, linear range, and detection limit (S/N = 3) are summarized in Table 1. As is listed, with increasing amount of loaded CuO NPs on GO sheet (from S_1 to S_3), the sensitivity gradually increases, the correlation coefficient becomes better, the linear range gradually is expanded, while the detection limit has little change. Taking all of these factors together, CuO/GO/GCE based on S_3 is the best one in this work, which saturated loads the CuO NPs on the GO sheets. Table 2 shows a comparison of the CuO/GO/GCE based on S_3 with some of the reported non-enzymatic glucose biosensors based on CuO or graphene hybrids. From a comparison, our sensor exhibits a satisfactory integrative performance that has the characteristics of high sensitivity, low detection limit, and large liner range. In particular, its sensitivity is much higher than those of the other sensors.

Table 1. Sensing Properties of Different Electrodes

	sensitivity, μA mM^{-1} cm^{-2}	R^2	linear range	detection limit, μM
S_1	137.60	0.9196	0.81 μM to 1.03 mM	0.33
S_2	195.98	0.9950	1.18 μM to 1.83 mM	0.44
S_3	262.52	0.9962	2.79 μM to 2.03 mM	0.69
S_3 in serum	285.38	0.9914	2.55 μM to 0.5 mM	0.69
CuO NPs (120 °C)	110.27	0.9998	0.77 μM to 2.03 mM	0.21

Moreover, to further investigate the nonenzymatic glucose sensing ability in real human blood, the $I-t$ curves of CuO/GO/GCEs based on S_3 by addition of human serum containing 50 μM glucose were carried out. As can be seen in Figure 7c, the current response is quite steady and fast with each addition of serum in the studied range. The corresponding calibration curve is shown in Figure 7d. The sensor displays a linear range from 2.55 μM to 0.5 mM human serum with a correlation coefficient of 0.9914, a sensitivity of 285.38 μA mM^{-1} cm^{-2}, and a detection limit of 0.69 μM (S/N = 3), as listed in Table 1. Since the nonenzymatic glucose sensors need to work under NaOH solution (0.1 M, pH 13), the real human serum will be diluted at least 100 times after injection into NaOH solution, and the linear range is enough to detect the concentration of glucose in human serum. Those data indicate that our sensor has great potential in clinical glucose detection. Note that the sensitivity in serum is a little higher than the sensitivity in pure glucose and this can be attributed to the influence brought by ascorbic acid (AA), uric acid (UA), and other compounds.

For the enhanced nonenzymatic glucose performance of CuO/GO/GCE in our work, two factors need to be considered: On the one hand, CuO NPs are a sensitive source for nonenzymatic glucose sensing in CuO/GO/GCE, as proved in Figure 5. Since the GO sheets exhibit high surface area, compared to the pure CuO/GCEs, the CuO NPs dispersed on GO sheets will have better dispersion and less agglomeration; thus, the effective area of CuO NPs can be more exposed to glucose molecules and then further improve the nonenzymatic

Table 2. Comparison between Our Sensor and the Previous Studies

electrode	detection potential	sensitivity	linear range	detection limit	ref
CuO/GO/GCE	+0.7 V	262.52 μA mM^{-1} cm^{-2}	2.79 μM to 2.03 mM	0.69 μM	this work
Cu nanoclusters	+0.65 V	17.76 μA mM^{-1}	1 μM to 5 mM	0.5 μM	29
CuO nanowires	+0.33 V	0.49 μA μM^{-1}	0.4 μM to 2 mM	0.049 μM	30
PdNP−graphene	+0.4 V		10 μM to 5 mM	1 μM	31
PtNi nanoparticle−graphene	−0.35 V	20.42 μA mM^{-1} cm^{-2}	up to 35 mM		32
3D graphene−cobalt oxide	+0.58 V	3.39 mA mM^{-1} cm^{-2}	0.1−80 μM	25 nM	9

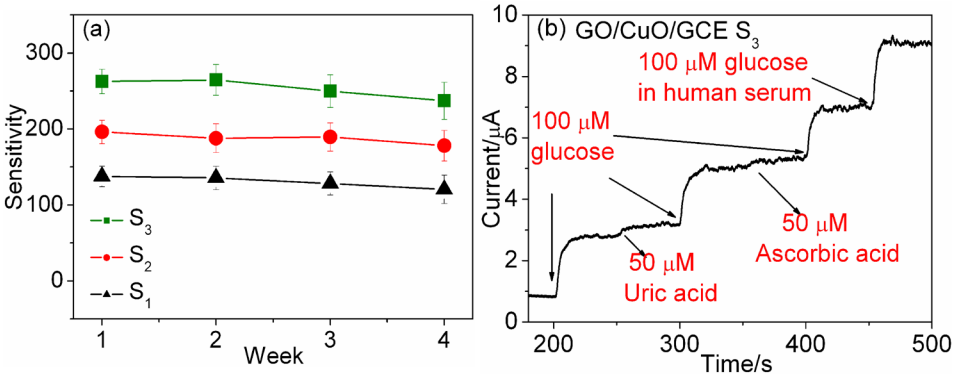

Figure 8. (a) Stability curves of S_1, S_2, and S_3. (b) Amperometric response of S_3 at 0.7 V with successive additions of different analytes.

glucose sensing performance in CuO/GO/GCE. However, the amount of loaded CuO NPs should be enough; otherwise, it will negatively affect the sensing performance (such as CuO/GO/GCE based on S_1). On the other hand, because of synergistic effect of the CuO NPs and GO sheets in CuO/GO composite, the excellent electric conductivity inherent in properties of GO sheets also makes a contribution.[33]

3.4. Reproducibility, Stability, Anti-Interference Property, and Real Sample Detection of the CuO/GO/GCE. To further confirm the nonenzymatic glucose performance, the reproducibility and stability of CuO/GO/GCEs were measured. For reproducibility, five CuO/GO/GCEs for each CuO/GO sample were separately prepared under the same conditions, the relative standard deviations (RSDs) were calculated to be no more than 5.4% (data is not shown), indicating a good reproducibility. The stability of CuO/GO/GCEs was tested once per week in 0.1 M NaOH at room temperature. As shown in Figure 8a, the decreases in sensitivity for CuO/GO/GCEs based on S_1, S_2, and S_3 after 4 weeks are no more than 9.7%, 9.2%, and 12.5%, respectively, indicating a good stability of CuO/GO/GCEs.

Anti-interference property is an important parameter for glucose sensors. Since human blood always containing many compounds like AA and UA and they are easy to be oxidized, the influence cannot be ignored. Generally, the concentration for healthy human is about 0.125 and 0.33 mM.[34,35] According to the previous research, the concentration of glucose in human blood is at least 10 times higher than that of the interfering species. The interference experiment of CuO/GO/GCEs based on S_3 was carried out with the addition of 100 μM glucose and 50 μM AA and UA, as shown in Figure 8b. Compared to glucose, the current responses of interfering species are 10.8% (50 μM UA) and 7.2% (50 μM AA) at +0.7 V. It can be concluded that the interference of small amount of AA and UA is very small. Moreover, for real sample detection, 100 μM glucose in human serum was also added after addition of glucose and interfering species in the anti-interference test, as shown in Figure 8b. After addition of 100 μM human serum glucose, an obvious current response can be observed. The concentration of glucose in the serum sample was calibrated by the Accu-Chekabtive glucose meter (OLYMPUSAU 400). As presented in Table 3, the results from the biosensor are similar to those tested by the glucose meter, indicating that the as-prepared biosensor may hold potential in real sample analysis.

Table 3. Glucose Concentration in Human Blood Serum Sample Measured by the Accu-Chekabtive Glucose Meter and Our GO/CuO/GCE

reading (mM)		
glucose meter	our sensor	RSD (%)
6.44	6.85	6.4

4. CONCLUSIONS

We synthesized a series of CuO/GO composites as well as monoclinic CuO NPs through a hydrothermal procedure. The influence of hydrothermal temperature, GO sheet, and loading amount of CuO on particle size and structure of CuO was systemically investigated. It was interesting to observe that the optimum hydrothermal temperature for the formation of pure monoclinic CuO was 120 °C. The existence of GO sheets could partly prevent the growth of the CuO NPs and was helpful to their monodispersion. The as-prepared samples were used to construct nonenzymatic glucose sensors. The optimal CuO/GO composites is S_3, which presents high sensitivity and a larger linear range compared to the other samples and also showed strong stability, good reproducibility, excellent selectivity, and accurate measurement in real serum sample. Moreover, it was used to detect the real human serum samples. The improved sensing properties for CuO/GO could be attributed to the increase of electroactive surface area of CuO NPs on GO sheets and the synergistic effect of CuO NPs and GO. Overall, according to the electrochemical measurements,

the CuO/GO/GCEs exhibit great potential for the application of nonenzymatic glucose biosensor.

■ ASSOCIATED CONTENT

Supporting Information

TEM images of CuO NPs synthesized at 150 and 180°C; CV curves of CuO/GO composites S_1 and S_2 based electrode before (black trace) and after (red trace) the injection of 5 mM glucose; and amperometric response of CuO NPs synthesized at 120, 150, and 180°C and the corresponding calibration curves. This material is available free of charge via the Internet at http://pubs.acs.org.

■ AUTHOR INFORMATION

Corresponding Authors

*L.X.: e-mail, linxu@jlu.edu.cn.

*H.S.: e-mail, songhw@jlu.edu.cn; phone and fax, 86-431-85155129.

Notes

The authors declare no competing financial interest.

■ ACKNOWLEDGMENTS

This work was supported by National Talent Youth Science Foundation of China (Grant 60925018), the National Natural Science Foundation of China (Grants 61204015, 51002062, 11174111, 61177042, and 81201738), the China Postdoctoral Science Foundation Funded Project (Grants 2012M511337 and 2013T60327), the Open Research Fund of State Key Laboratory of Bioelectronics, Southeast University, and the Open Fund of the State Key Laboratory on Integrated Optoelectronics Grant IOSKL2012KF04.

■ REFERENCES

(1) Mitro, N.; Mak, P. A.; Vargas, L.; Godio, C.; Hampton, E.; Molteni, V.; Kreusch, A.; Saez, E. *Nature* **2007**, *445*, 219−223.
(2) Shi, J.; Zhang, H. Y.; Snyder, A.; Wang, M. X.; Xie, J.; Porterfield, D. M.; Stanciu, L. A. *Biosens. Bioelectron.* **2012**, *38*, 314−320.
(3) Huang, Y.; Dong, X.; Shi, Y.; Li, C. M.; Li, L. J.; Chen, P. *Nanoscale* **2010**, *2*, 1485−1488.
(4) Song, Y.; Qu, K.; Zhao, C.; Ren, J.; Qu, X. *Adv. Mater.* **2010**, *22*, 2206−2210.
(5) Gouda, M. D.; Singh, S. A.; Rao, A. G. A.; Thakur, M. S.; Karanth, N. G. *J. Biol. Chem.* **2003**, *278*, 24324−24333.
(6) Forzani, E. S.; Zhang, H.; Nagahara, L. A.; Amlani, I.; Tsui, R.; Tao, N. *Nano Lett.* **2004**, *4*, 1785−1788.
(7) Yang, W.; Ratinac, K. R.; Ringer, S. P.; Thordarson, P.; Gooding, J. J.; Braet, F. *Angew. Chem., Int. Ed.* **2010**, *49*, 2114−2138.
(8) Pang, H.; Lu, Q.; Wang, J.; Li, Y.; Gao, F. *Chem. Commun.* **2010**, *46*, 2010−2012.
(9) Dong, X. C.; Xu, H.; Wang, X. W.; Huang, Y. X.; Chan-Park, M. B.; Zhang, H.; Wang, L. H.; Huang, W.; Chen, P. *ACS Nano* **2012**, *6*, 3206−3213.
(10) Li, C.; Liu, Y.; Li, L.; Du, Z.; Xu, S.; Zhang, M.; Yin, X.; Wang, T. *Talanta* **2008**, *77*, 455−459.
(11) Shamsipur, M.; Najafi, M.; Hosseini, M. R. M. *Bioelectrochemistry* **2010**, *77*, 120−124.
(12) Kim, K. S.; Zhao, Y.; Jang, H.; Lee, S. Y.; Kim, J. M.; Ahn, J. H.; Kim, P.; Choi, J. Y.; Hong, B. H. *Nature* **2009**, *457*, 706−710.
(13) Geim, A. K.; Novoselov, K. S. *Nat. Mater.* **2007**, *6*, 183−191.
(14) Novoselov, K. S.; Geim, A. K.; Morozov, S. V.; Jiang, D.; Zhang, Y.; Dubonos, S. V.; Grigorieva, I. V.; Firsov, A. A. *Science* **2004**, *306*, 666−669.
(15) Liu, Y.; Dong, X.; Chen, P. *Chem. Soc. Rev.* **2012**, *41*, 2283−2307.
(16) Jiang, H. *Small* **2011**, *7*, 2413−2427.
(17) Sun, X.; Liu, Z.; Welsher, K.; Robinson, J. T.; Goodwin, A.; Zaric, S.; Dai, H. *Nano Res.* **2008**, *1*, 203−212.
(18) Li, X. R.; Kong, F. Y.; Liu, J.; Liang, T. M.; Xu, J. J.; Chen, H. Y. *Adv. Funct. Mater.* **2012**, *22*, 1981−1988.
(19) Claussen, J. C.; Kumar, A.; Jaroch, D. B.; Khawaja, M. H.; Hibbard, A. B.; Porterfield, D. M.; Fisher, T. S. *Adv. Funct. Mater.* **2012**, *22*, 3399−3405.
(20) Luo, L.; Zhu, L.; Wang, Z. *Bioelectrochemistry* **2012**, *88*, 156−163.
(21) Meher, S. K.; Rao, G. R. *Nanoscale* **2013**, *5*, 2089−2099.
(22) Wang, H.; Casalongue, H. S.; Liang, Y.; Dai, H. *J. Am. Chem. Soc.* **2010**, *132*, 7472−7477.
(23) Kovtyukhova, N. I.; Ollivier, P. J.; Martin, B. R.; Mallouk, T. E.; Chizhik, S. A.; Buzaneva, E. V.; Gorchinskiy, A. D. *Chem. Mater.* **1999**, *11*, 771−778.
(24) Mai, Y. J.; Wang, X. L.; Xiang, J. Y.; Qiao, Y. Q.; Zhang, D.; Gu, C. D.; Tu, J. P. *Electrochim. Acta* **2011**, *56*, 2306−2311.
(25) Wang, X.; Hu, C.; Liu, H.; Du, G.; He, X.; Xi, Y. *Sens. Actuators, B* **2010**, *144*, 220−225.
(26) Zhao, Y.; Song, X.; Song, Q.; Yin, Z. *CrystEngComm* **2012**, *14*, 6710−6719.
(27) Zhou, M.; Zhai, Y. M.; Dong, S. J. *Anal. Chem.* **2009**, *81*, 5603−5613.
(28) Xu, Q.; Zhao, Y.; Xu, J. Z.; Zhu, J. J. *Sens. Actuators, B* **2006**, *114*, 379−386.
(29) Kang, X.; Mai, Z.; Zou, X.; Cai, P.; Mo, J. *Anal. Biochem.* **2007**, *363*, 143−150.
(30) Zhuang, Z.; Su, X.; Yuan, H.; Sun, Q.; Xiao, D.; Choi, M. M. F. *Analyst* **2008**, *133*, 126−132.
(31) Lu, L. M.; Li, H. B.; Qu, F.; Zhang, X. B.; Shen, G. L.; Yu, R. Q. *Biosens. Bioelectron.* **2011**, *26*, 3500−3504.
(32) Gao, H.; Xiao, F.; Ching, C. B.; Duan, H. *ACS Appl. Mater. Interfaces* **2011**, *3*, 3049−3057.
(33) Wang, B.; Wu, X. L.; Shu, C. Y.; Guo, Y. G.; Wang, C. R. *J. Mater. Chem.* **2010**, *20*, 10661−10664.
(34) Park, S.; Boo, H.; Chung, T. D. *Anal. Chim. Acta* **2006**, *556*, 46−57.
(35) Hrapovic, S.; Luong, J. H. T. *Anal. Chem.* **2003**, *75*, 3308−3315.